Indigenous equipments and Pressure devices developed at CHPR and the technical details are follows:

High pressure physics has been emerging field in recent years with the combination of high pressure devices with advancement in the probing techniques for the investigation of new materials. In the above context, we developed the following pressure cells and devices to explore the mechanism of various exotic phenomena such as superconductivity, Charge Density Wave (CDW), magnetocaloric effect, magnetoresistance effect, etc., in the light of high pressure physics. Hence, the nominee, Dr. S. Arumugam has developed various indigenous instruments such as: **1)** Uniaxial pressure device for electrical resistivity measurements suitable for closed cycle refrigerator system; **2)** Uniaxial pressure device for ac-susceptibility measurements suitable for closed cycle refrigerator system; **3)** Uniaxial pressure device for magnetization measurements suitable for PPMS-VSM; **4)** A DC-SQUID vibrating coil magnetometer for the magnetic measurements of extremely small volume of samples; 5) Hydrostatic pressure cell (~ 3.5 GPa) for electrical resistivity measurements suitable for CCR-VTI and PPMS; 6) Bridgman anvil quasi-hydrostatic pressure cell (~8 GPa) for electrical resistivity measurements suitable for CCR-VTI and PPMS;7) Modified Bridgman anvil hydrostatic pressure cell (~8 GPa) for electrical resistivity measurements suitable for CCR-VTI; 8) Diamond Anvil Pressure cell (~20 GPa) for electrical resistivity measurements suitable for CCR-VTI and PPMS (under optimization); 9) Uniaxial pressure device for electrical resistivity measurements suitable for 17 Tesla superconducting magnet system.

Hydrostatic pressure techniques:

Piston-cylinder hydrostatic pressure cell ~1 GPa: magnetic measurements suitable for PPMS – VSM System: (M-cell and indigenously designed & fabricated at CHPR).

The body of the pressure cell is made of especially heat treated nonmagnetic Cu- Be alloy. To perform the temperature dependence of magnetization measurements under various fixed pressures, the sample of ~ 10 mg and calibrant (Sn) are kept inside a Teflon capsule. The liquid pressure-transmitting medium of Fluorinert #70: Fluorinert #77 in 1:1 ratio is filled in the Teflon capsule and closed with Teflon cap.

The capsule and other components are assembled in the pressure cell. Required pressure is applied and clamped using a 20 ton hydraulic press (M/s Reiken Kiki Co Ltd, Japan). In-situ pressure calibration is carried out with the change of TC of Sn which is kept

along with the sample in the Teflon capsule. The pressure cell is then inserted into the PPMS dewar through the VSM linear motor. We have investigated temperature and field dependence of magnetization measurements at various fixed pressures for various materials such as superconductors, heavy fermions, Heusler alloys, manganites, Dirac metals etc. using this hydrostatic pressure cell up to 1 GPa, temperature 2- 400 K and 9 T magnetic field. Figure 1 shows (a) Photograph of a hydrostatic pressure cell (1 GPa) (Mcell-10, EasyLab, UK) with its components; (b) Photograph of a assembly of pressure cell components developed at CHPR; (c-e) Pressure cell calibration data.

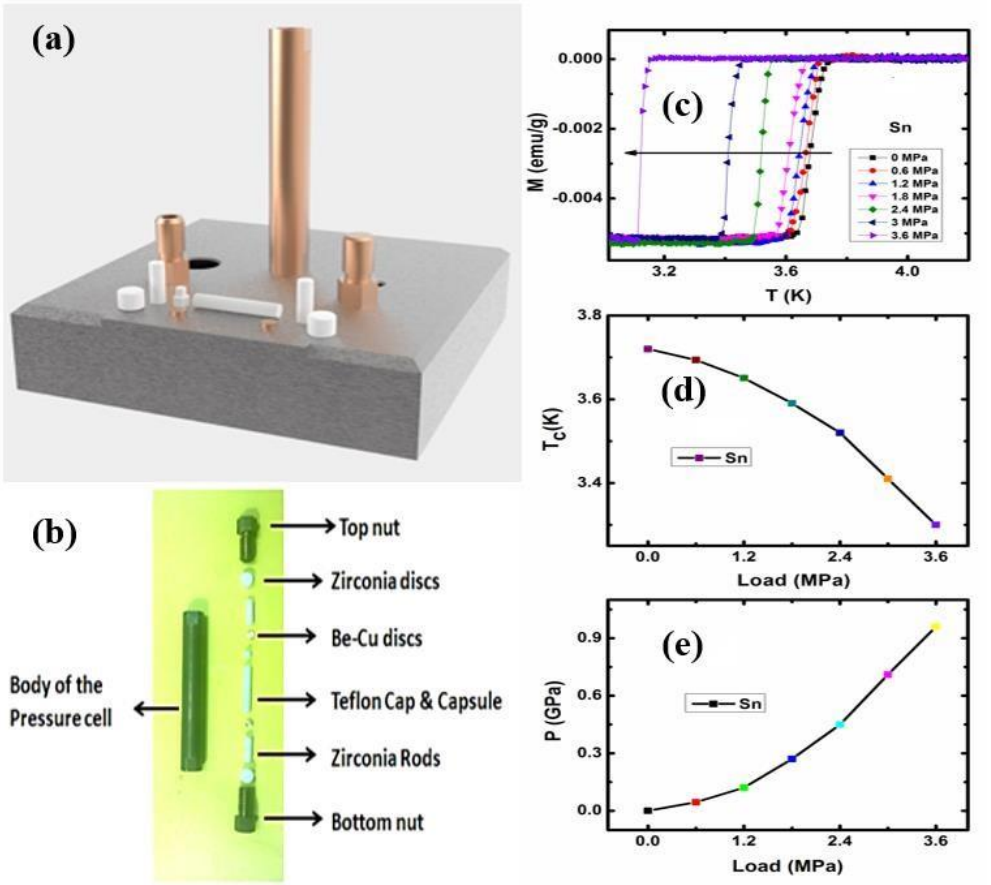

Figure:1. (a) Photograph of a hydrostatic pressure cell (1 GPa) (Mcell-10, Easy Lab, UK) with its components; (b): Photograph of a assembly of pressure cell components developed at CHPR; (c-e) Pressure cell calibration data.

Piston-cylinder hydrostatic pressure cell (3 GPa): Suitable for Closed Cycle Refrigerator – Variable Temperature Insert (CCR-VTI) and PPMS system.

This pressure cell can generate pressure up to a maximum limit of 3 GPa. The outer cylinder (body of the cell) and inner cylinder is made of Be (2%)-Cu alloy and hardened stainless steels alloy respectively.

The sample is kept inside a Teflon capsule (obturator) which is filled with pressure transmitting medium (Daphne # 7474). The pressure cell is calibrated with structural phase transitions of Bi (I-II at 2.55 GPa and II-III at 2.77 GPa) at room temperature using 20 ton hydraulic press (M/s Reiken Kiki Co Ltd, Japan). The required pressure is clamped in the pressure cell at room temperature and transferred to PPMS puck for electrical resistivity measurements. Figure 2 shows Photograph of (a) a piston-cylinder hydrostatic pressure cell (~3 GPa): Suitable for CCR -VTI and PPMS; (b) 3D view of piston-cylinder hydrostatic pressure cell; (c) Photograph of two samples mounted in the obturator; (d) Resistance vs applied load (MPa); (e) Pressure calibration curve: actual pressure (GPa) vs applied Load (MPa) of the Bi at room temperature.

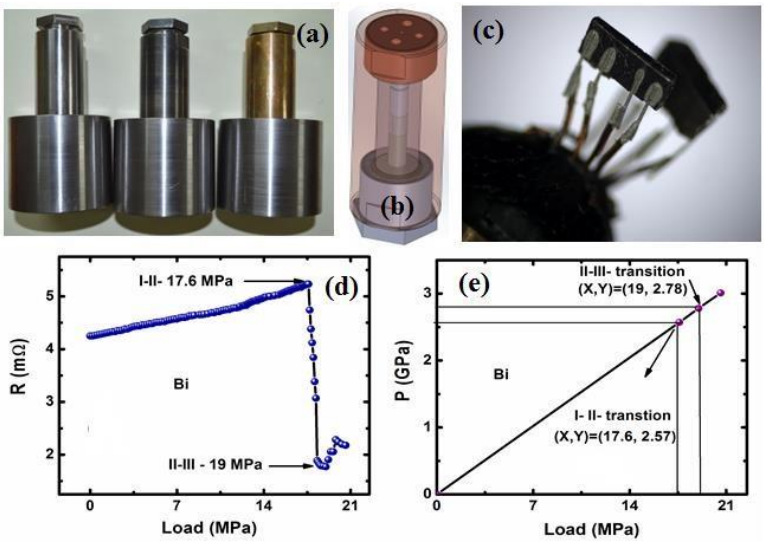

Figure 2. Photograph of (a) a piston-cylinder hydrostatic pressure cell (~3 GPa): Suitable for Closed Cycle Refrigerator System - Variable Temperature Insert module and PPMS; (b) 3D view of piston-cylinder hydrostatic pressure cell; (c) Photograph of two samples mounted in the obturator; (d) Resistance vs applied load (MPa); (e) Pressure calibration curve: actual pressure (GPa) vs applied Load (MPa) of the Bi at room temperature.

High pressure hybrid clamp type piston - cylinder pressure cell (3.5 GPa): Suitable for Closed Cycle Refrigerator – Variable Temperature Insert (CCR-VTI) and PPMS system.

The pressure cell is designed and fabricated suitable for the commercially available both CCR-VTI and PPMS systems. Both outer (body of the cell) and inner cylinders are made of hardened stainless steels alloys. The sample is kept inside a Teflon cap (obturator) which is

filled with pressure transmitting medium (Daphne # 7474). The pressure cell is calibrated with structural phase transitions of Bi (I-II at 2.55 GPa and II- III at 2.77 GPa) at room temperature using 20 ton hydraulic press (M/s Reiken Kiki Co Ltd, Japan). The required pressure is clamped at room temperature and transferred to CCR-VTI/PPMS system for electrical resistivity measurements. This pressure cell can generate pressure up to a maximum limit of ~ 3.5 GPa.

Figure 3. shows the photograph of (a) High pressure hybrid clamp type piston - cylinder pressure cell (3.5 GPa) with the pressure push rod assembly: Suitable for both CCR-VTI and PPMS systems; (b) P cell developed at CHPR on different materials; (b) Resistance vs applied load (MPa); (d) Pressure calibration curve: actual pressure (GPa) vs applied Load (MPa) of the Bi at room temperature. Furthermore, Figure 4 indicates the photographs of two samples mounted in the obturator used for the ρ(T) measurements.

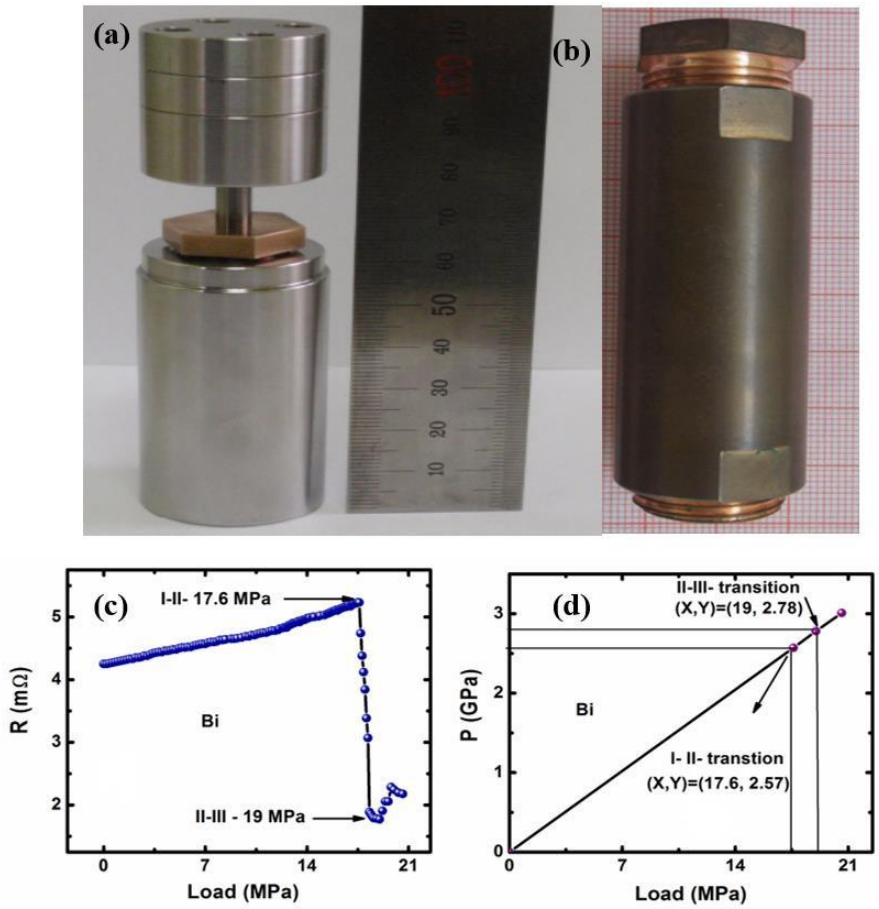

Figure 3: Photograph of (a) High pressure hybrid clamp type piston - cylinder pressure cell (3.5 GPa) with pressure push rod assembly: Suitable for Closed Cycle Refrigerator – Variable Temperature Insert (CCR-VTI) and PPMS system; (b) P cell developed at CHPR on different materials; (c) Resistance vs applied load (MPa); (d) Pressure calibration curve: actual pressure (GPa) vs applied Load (MPa) of the Bi at room temperature

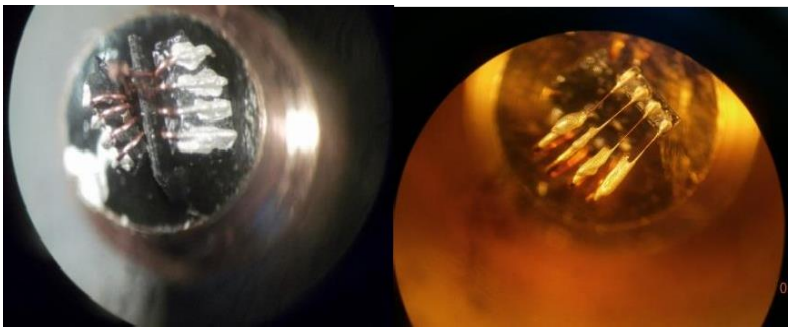

Figure 4: Photograph of two samples mounted in the obturator.

Modified Bridgman anvil hydrostatic pressure cell (~ 8 GPa): Suitable for CCR-VTI

Recently, we have developed the modified Bridgman anvil hydrostatic pressure cell, which is equivalent to cubic press system to do electrical resistivity measurements and calibrated at room temperature up to 8 GPa and this pressure cell suits for CCR-VTI. It has been developed in collaboration with Prof. Y. Uwatoko, Institute for Solid State Physics, University of Tokyo, Japan. The description of the MB anvil as follows. The most important feature of this pressure cell is its compact body and its size is slightly larger than conventional clamp type hybrid piston cylinder hydrostatic P cell.

The body of the cell is made of specially heat treated CuBe with an outer diameter of 38 mm. Required load is applied to the anvils via the WC piston by a 100 ton hydraulic press at room temperature and clamped by the CuBe top nut. The sample is set in the Teflon capsule and filled with daphne # 7474 as a pressure transmitting medium in order to generate a nearly hydrostatic condition. Au foil thickness of 20 μm and the Au wires (10 μm) are used to connect the sample electrically to each stainless steel plates with thicknesses of 0.15 mm. The dimensions of the sample are 0.7 X 0.4 X 0.1mm^3. Figure 5 shows (a) Photograph of assembled MB-Anvil pressure cell with holder; (b) 3D view of MB-Anvil pressure cell; (c) Cross-sectional and bottom view of the MB anvil pressure cell and its components; (d) Photograph of the sample assembly; (e) Electrical resistivity under various P up to 8 GPa for $BiSbTe_{1.25}Se_{1.75}$.

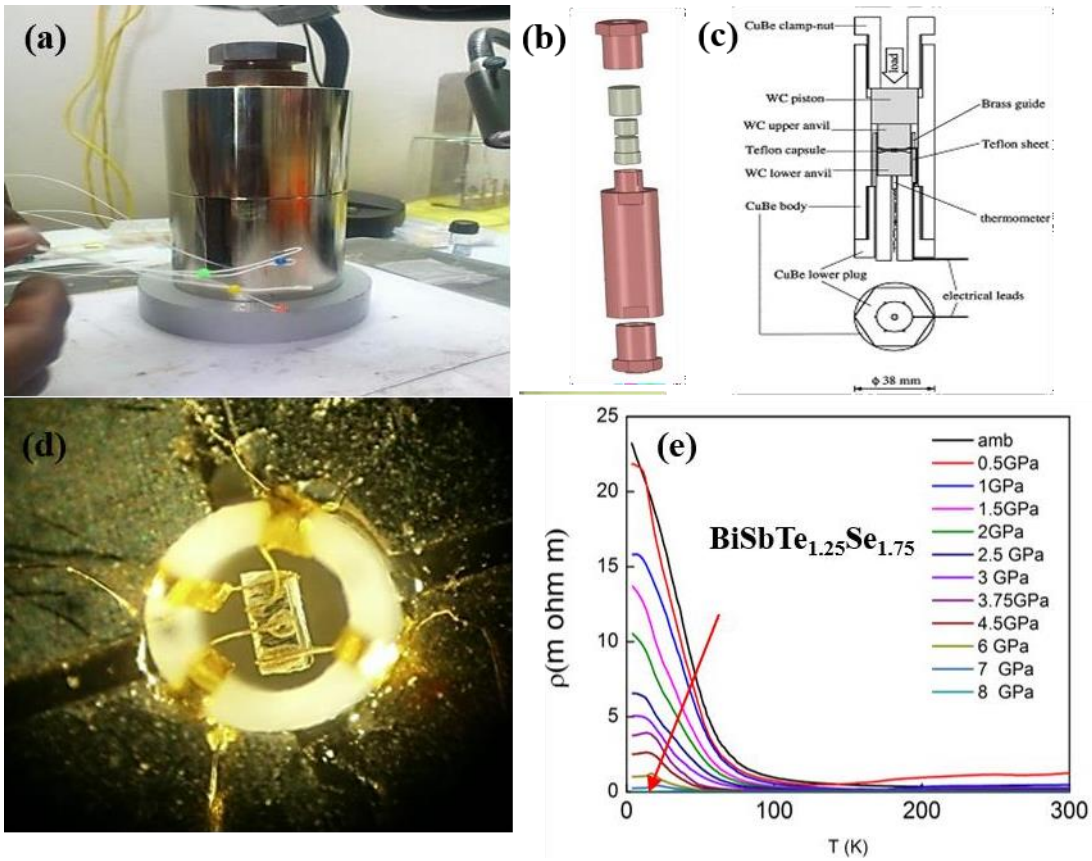

Figure 5: (a) Photograph of assembled MB-Anvil Pressure cell with holder; (b) 3D view of MB-Anvil pressure cell; (c) Cross-sectional and bottom view of the MB anvil pressure cell and its components; (d) Photograph of the sample assembly; (e) Electrical resistivity under various P up to 8 GPa for $BiSbTe_{1.25}Se_{1.75}$.

The applied pressure is calibrated with Bi using 100 ton hydraulic press and it is similar to pressure calibration in cubic anvil press at room temperature up to ~ 8 GPa, shown in figure 6 (a, b). The structural phase transitions of Bi-I-II at 2.55 GPa, II-III at 2.77 GPa and III-IV at ~7.68 GPa were observed in the P versus Load curve.

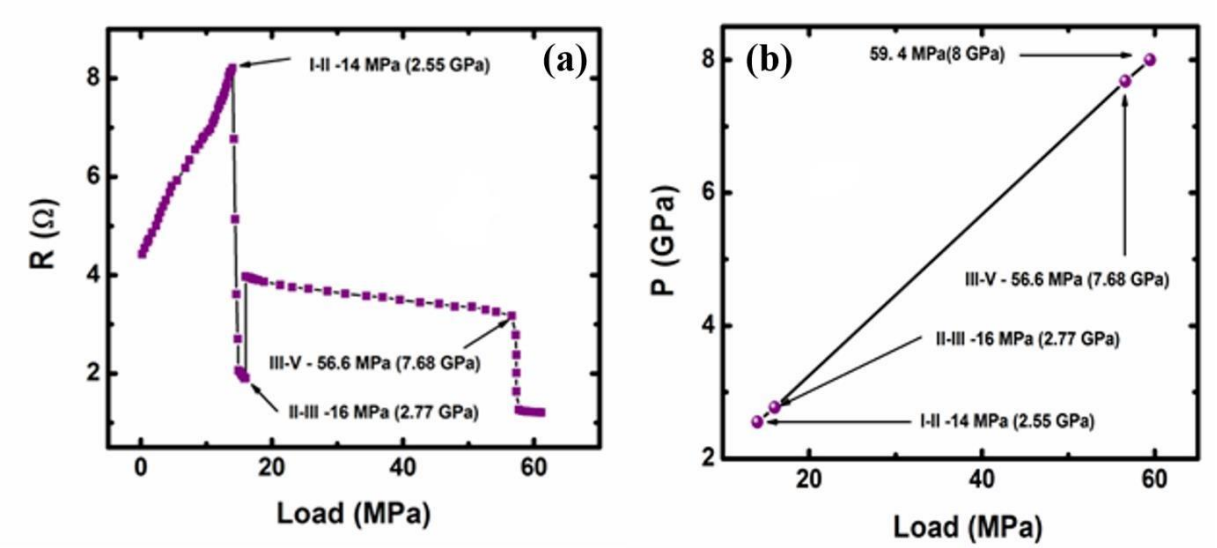

Figure 6: (a) Resistance (R) vs Load (MPa) of Bismuth (Bi) at room temperature. (b) The structural phase transitions of Bi-I-II at 2.55 GPa, II-III at 2.77 GPa and III-IV at ~7.68 GPa were observed in the P versus Load curve.

Quasi-Hydrostatic pressure techniques

Quasi-Hydrostatic Bridgman Anvil pressure cell (~ 8 GPa): Suitable for CCR-VTI

We designed and fabricated two different sizes (35 mm ϕ and 45 mm ϕ) of clamp type Bridgman Anvil Pressure cells suitable for existing CCR-VTI to do electrical resistivity measurements upto 8 GPa for metallic and alloys samples only. The pressure cells with the 35 mm ϕ and 45 mm ϕ are expected to reach ~ 8 GPa and ~ 9 GPa respectively.

The pressure cell is integrated with the CCR-VTI and resistivity measurements is optimized at room temperature for various fixed pressures. The pressure cells are made of the hardened SS alloys (outer cylinder, top nut, bottom nut and supporting ring) except Tungsten Carbide anvil. The hardened SS alloys are specially heat treated in different atmosphere and optimized with the measurement of grain size and hardness to suit for a pressure cell. We used tungsten carbide as an anvil with 6 mm face diameter, pyrophyllite as the gaskets and Aluminium Magnesium silicate ($AlMgO_3Si$) as a pressure transmitting medium. We used four probe method to carry out the electrical resistivity measurements and calibrated at RT temperatures. Figure 7 shows (a) Photograph of the Bridgman Anvil Pressure cell; (b) 3D view of Bridgman-Anvil P cell with bottom holder and pressure application rod; (c) 3D view of Bridgman Anvil P cell (d) Resistance (R) vs Load (PSI) of Bismuth (Bi) at RT; (e) The

structural phase transitions of Bi-I-II at 2.55 GPa, II-III at 2.77 GPa and III-IV at ~7.68 GPa were observed at RT in the P versus Load (PSI) curve.

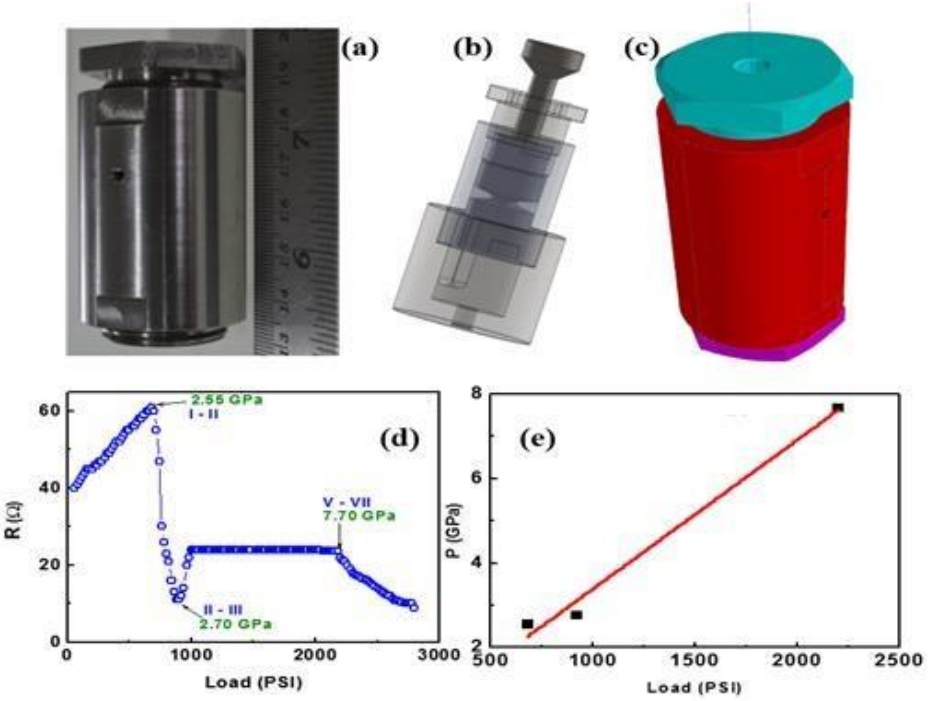

Figure 7: (a) Photograph of the Bridgman Anvil Pressure cell; (b) 3D view of Bridgman-Anvil P cell with bottom holder and top pressure application rod; (c) 3D view of Bridgman Anvil P cell (d) Resistance (R) vs Load (PSI) of Bismuth (Bi) at RT; (e) The structural phase transitions of Bi-I-II at 2.55 GPa, II-III at 2.77 GPa and III-IV at ~7.68 GPa were observed at RT in the P versus Load (PSI) curve.

Diamond Anvil cell (20GPa): Suitable for PPMS and CCR-VTI System:

Diamond Anvil pressure cell is designed and fabricated for doing electrical resistivity measurements down to 2 K. The pressure cell is made of the hardened SS alloys (Figure 8a). The hardened SS alloy is specially heat treated in specific atmosphere and optimized with the

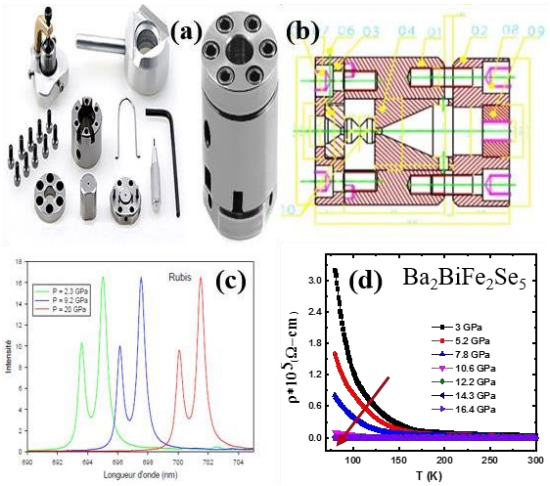

Figure 8: (a) Photographs of Diamond Anvil cell with components suitable for PPMS and CCR-VTI System; (b) 2D diagram of Diamond Anvil Cell; (c) Ruby fluorescence calibrated data; (d) ρ(T) under various P up to 16.4 GPa for $Ba_2BiFe_2Se_5$.

measurement of grain size and hardness. We used diamond as an anvil with 0.5mm/1 mm size

culet diameter and 3.5mm diameter table size and 300 µm thick stainless steel (SS) gasket. The pressure cell (DAC) suits for existing 9 T PPMS and CCR –VTI and R(T) measurements under optimization including calibration of pressure at RT. Figure 8 shows (a) Photographs of Diamond Anvil cell with components suitable for CCR-VTI System and PPMS; (b) 2D diagram of Diamond Anvil Cell; (c) Ruby fluorescence calibrated data; (d) R(T) under various P upto 16.4 GPa for $Ba_2BiFe_2Se_5$.

The Ruby pressure calibration setup includes recent Olympus industrial microscope, high resolution and high stable CCD spectrometer (range: 690-870 nm) and Ruby pressure calibration software with a laptop is shown in Figure 9 (b). The micro drilling machine based on the principle of Electrical discharge machining (EDM) which can drill SS gasket from 20 µm ϕ to 1000 µm ϕ with the thickness of 500 µm in a perfect round shape.

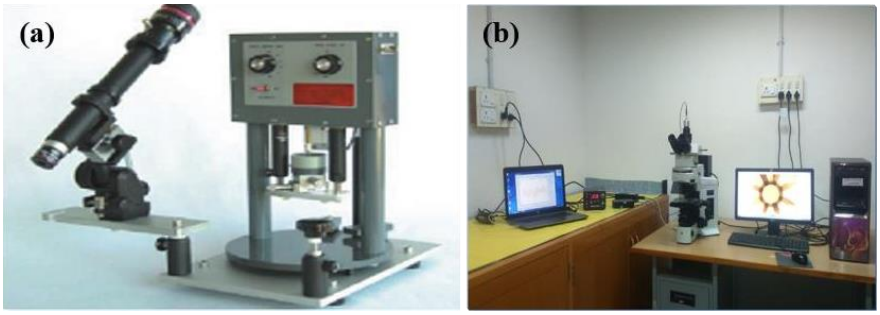

Figure 9: Photograph of (a) micro drilling machine; (b) Ruby fluorescence P calibration setup.

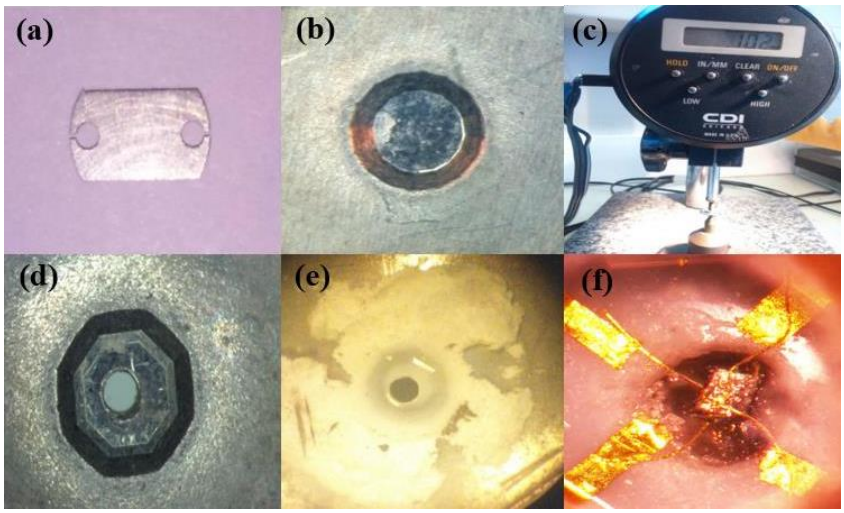

Figure10: A photograph of (a) 300µm SS gasket; (b) A indented SS gasket; (c) A micrometer; (d) A drilled SS gasket; (e) Photograph of insulated gasket; (b) A sample assembly in DAC gasket

Uniaxial Pressure Techniques

A simple uniaxial pressure device for electrical resistivity measurements: Suitable for closed cycle refrigerator system – Cold Head model.

A simple uniaxial pressure device suitable for closed cycle refrigerator system (CCRS) has been built (Figure 11). This device in principle is applicable to any crystal. In this device the pressure can be varied smoothly and continuously to any desired temperature using a disc-micrometer and a spring – holder attachment, which are kept on the demountable top flange of the vacuum shroud of CCRS at room temperature.

This device is not dependent on pressure calibration and the pressure calculation is obtained directly from the surface area of the crystal, the rotations of the disc- micrometer and the spring – constant value of the spring. Piezoresistance measurements were made on n-type Si to check the quality of data from the uniaxial pressure device.

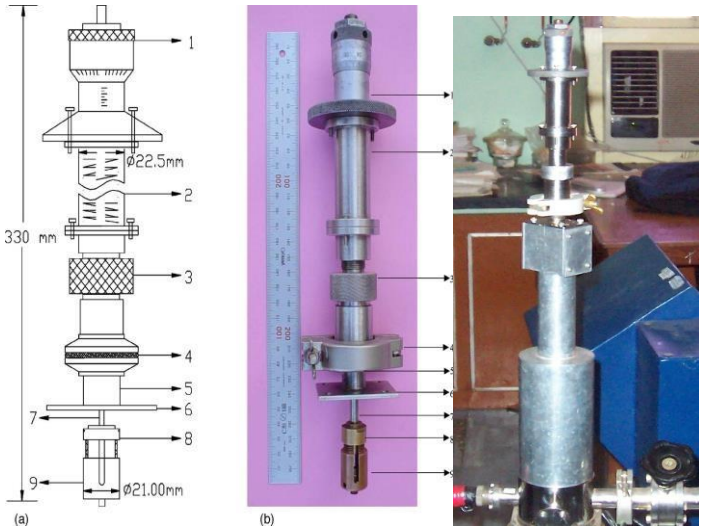

Figure 11: (a) Mechanical diagram (front view) of the uniaxial pressure device; (b) Photograph of a uniaxial pressure device (front view); (c) Cold Head with uniaxial pressure device.

Figure 12: Temperature dependence of resistivity at various pressures (a) || to ab plane of (b)

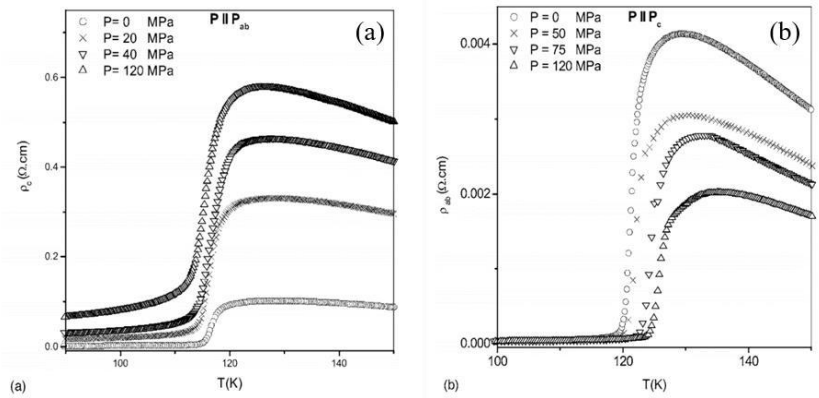

|| to c axis, LSMO single crystal

The performance of the uniaxial pressure device is illustrated by investigating the uniaxial pressure dependence of various strongly correlated materials such as $La_{1.48}Nd_{0.4}Sr_{0.12}CuO_4$, $La_{1.4}5Nd_{0.4}Sr_{0.15}CuO_4$, $La_{1.85}Sr_{0.15}CuO_4$, $Sm_{1-x}Sr_xMnO_3$ (x=0.45), and $La_{1.25}Sr_{1.75}Mn_2O_7$ single crystals along the ab -plane and c-axis using electrical resistivity measurements down to 15 K.

Modified uniaxial pressure device for electrical resistivity measurements: Suitable for CCR-VTI

The uniaxial pressure cell and the anvils are made of hardened high purity Be (2%) - Cu alloy. Two slots are provided in the opposite side with 3.2 mm width and 24 mm length from the top of the pressure cell to the top of the bottom anvil. A hole of 2.5 mm ϕ is provided at the bottom of the pressure cell for the easy mounting and demounting of the anvil into the pressure cell. The electrical resistivity was measured using continuous variation uniaxial pressure experimental device is shown in figure 2.18. It is a direct uniaxial pressure method. The uniaxial pressure device consists of a 1) disc- micrometer 2) an SS spring holder and SS spring (3), SS extended guiding tube (4) a rubber O-ring (5) a uniaxial pressure cell holder & uniaxial pressure cell. The disc- micrometer (Mitutoyo, Japan), high strength steel spring with known spring constant and the SS spring holder comprise the force generator.

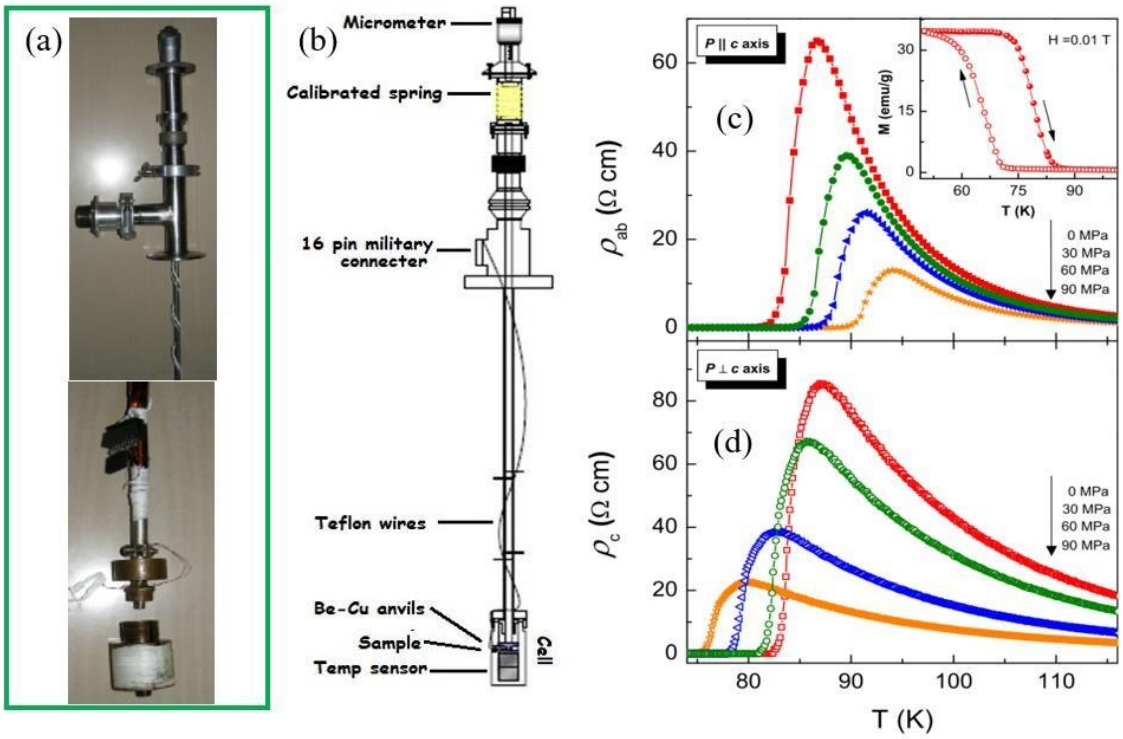

Figure 13: (a) Modified uniaxial pressure device suitable for CCR-VTI for electrical resistivity measurements (b) Schematic diagram of a Modified uniaxial pressure device; Temperature dependence of (c) ab-plane resistivity (ρab) of Sm0.55(Sr0.5Ca0.50)0.45MnO3 single crystal measured under various uniaxial pressures parallel to c axis (P∥c); (d) c- axis resistivity (ρc) measured for various pressures, applied perpendicular to the c axis (P⊥c) [Inset shows M (T) of both in heating and cooling cycles].

The spring is kept inside the SS spring holder and the maximum pressure generation may be varied by choosing a different spring – constant value of the spring. The pressure is applied through a force generator at room temperature by rotating the disc-micrometer for a specific value of pressure and transferred to the sample in pressure cell of CCR-VTI. Pressure is calculated directly by knowing the spring – constant value of the spring, the displacement in terms of micrometer rotations and the surface area of the single crystal on which pressure is applied. The normalized resistivity as a function of pressure for n- type Si along (100) planes at 300 K to cross check the pressure calibration. The applied pressure is maintained by the force generator at all temperatures ranging from 300 K to 4 K. The pressure cell is cooled more effectively through the exchange of helium gas in the cryostat chamber of CCR-VTI. In the present setup, it is possible to vary the pressure at room temperature after every set of ρ (T) without removing insert from the CCR-VTI.

A simple uniaxial pressure device for ac- susceptibility measurements: Suitable for CCR system (Cold Head model).

A simple design of uniaxial pressure device utilized for measurement of ac-susceptibility at low temperatures for the first time using closed cycle refrigerator system (CCRS) is developed and calibrated (Figure 13). This device mainly consists of disc-micrometer, spring – holder attachment, uniaxial pressure cell and the ac-susceptibility coil wounded on stycast former. The present device has many features: simple in design, failure of the coil is remote, inexpensive and no need for pressure calibrant. Also, it is easy to change the sample, calculation of pressure, pressure generation, performing experiment and comfortable for small samples.

It can be used under pressure upto 0.5 GPa and at temperatures from 30K to 300K. The system performance at ambient pressure is tested with calibration of standard paramagnetic salts (Gd_2O_3, Er_2O_3 and $Fe(NH_4SO_4)_2$ $6H_2O$), Fe_3O_4, Gd-metal, Dy-metal, superconductor ($YBa_2Cu_3O_7$), manganite ($La_{1.85}Ba_{0.15}MnO_3$) and spin glass material ($Pr_{0.8}Sr_{0.2}MnO_3$). The performance of the uniaxial pressure device is demonstrated by investigating the uniaxial pressure dependence of $La_{1.85}Ba_{0.15}MnO_3$ single crystal is shown in figure 14 (c).

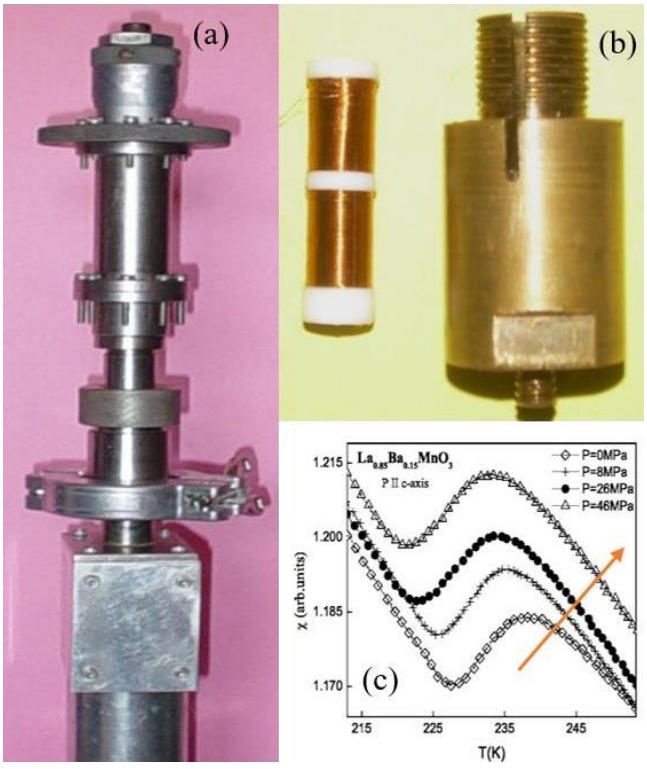

Figure 14: (a) Photograph of a uniaxial pressure device for ac-susceptibility measurements (front view); (b) Photograph of the pressure cell and coil. (c) Temperature dependence of ac susceptibility of $La_{0.85}Ba_{0.15}MnO_3$ single crystals at various uniaxial pressures (P∥c) axis near the metal-insulator transition.

Micro uniaxial Pressure cell for magnetization measurements:

We have fabricated a new clamp type micro-uniaxial pressure cell for DC susceptibility measurements is shown in figure 15 (a,b). The pressure cell can be used in the temperature range of 1.8 K to 400 K and suitable for Magnetic Property Measurement System (9T MPMS / PPMS-VSM, Quantum Design, USA). The pressure cell consists of top clamping bolt, bottom clamping bolt, body of the cell, spring, spring backup, spacer, push piston and piston backup. The body of the cell, lower and upper pressure clamping bolt, supporting cylinder and the spring are made of non-magnetic Be (2%)-Cu alloy and made suitable annealing to get maximum hardness with lowest magnetic moment at low temperature. The spring is kept at the top portion of the pressure cell with the spring backups. The push pistons are made of zirconia (Kyocera, Japan).

The pressure is applied and locked through an top clamping bolt of the pressure cell with a known fixed force. The maximum pressure can be applied upto 1.0 GPa and the maximum pressure can be varied based on the strength of the spring. The pressure is applied by digital torque wrench at room temperature, clamped and hangs into the holder of the MPMS to do M (T) measurements at low temperatures.

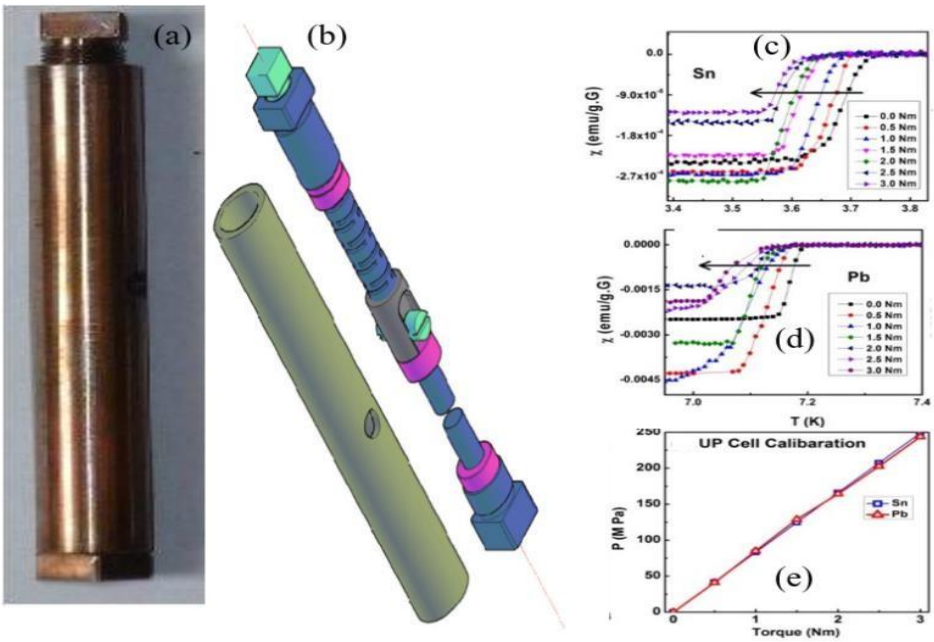

Figure 15: (a) Photograph of a micro uniaxial Pressure cell for magnetization measurements (1GPa): Suitable for MPMS and PPMS - VSM – system; (b) 3D view of the micro uniaxial Pressure cell; (c-e) Sn and Pb pressure calibration curves.

The pressure is calculated from the known applied force and the area of the sample kept in the pressure cell. Also, the pressure is calibrated by studying the pressure dependence

of superconducting transition temperature (TC) of Sn. The capability of our device is from 0 to 1.0 GPa. Performance of this device tested on various anisotropy spin ladder systems such as $Sr_3Ca_{11}Cu_24O_{41}$, $SrCa_{13}Cu_{24}O_{41}$, $Sr_{1.8}$ $Ca_{12.2}Cu_{24}O_{41}$, and $Sr_3Fe_2O_{6.75}$.

A SQUID vibrating coil magnetometer for the magnetic measurements of extremely small volume of samples

Superconducting Quantum Interference Device (SQUID) is the world's most sensitive detectors of weak magnetic signals and it has an ability to monitor extremely small changes in magnetic fields even in the presence of relatively large dc magnetic fields. We have developed a high sensitive magnetic measurement technique suitable for extremely small volume of samples using SQUID vibrating coil magnetometer (SVCM) and tested successfully. Such high sensitivity SVCM equipment was developed in collaboration with Materials Science Division, IGCAR, Kalpakkam and Centre for Cryogenic Technology, Indian Institute of Science, Bangalore. In this setup position differentiating detection (PDD) of magnetic flux

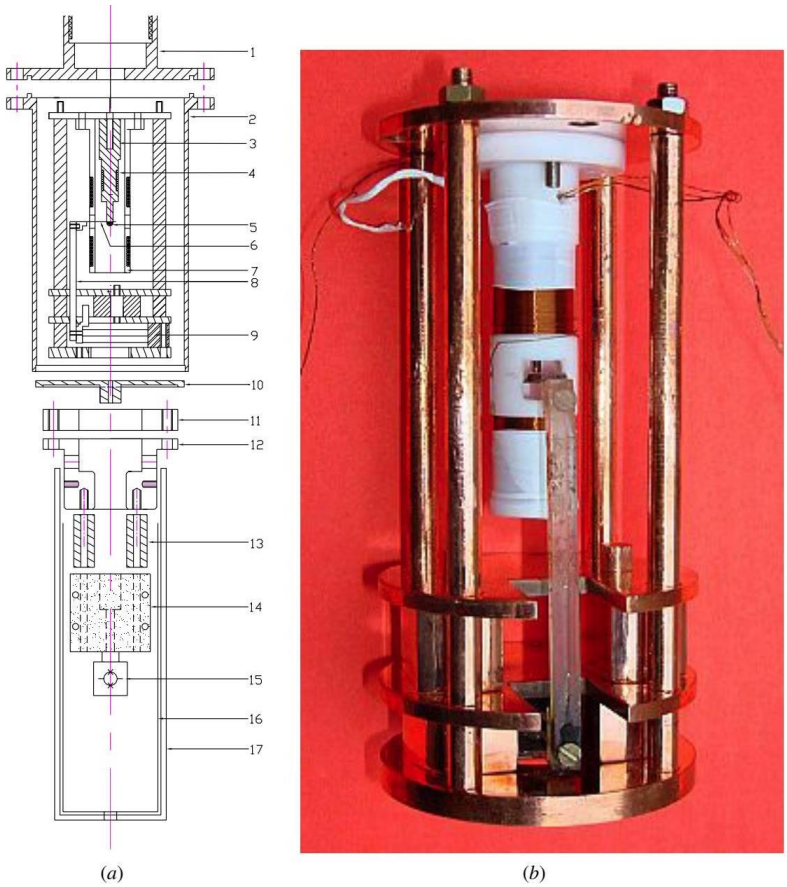

from the sample is combined with the use of SQUID magnetometer. The sensitivity of the setup depends on the vibrational amplitude of the pick-up coil.

Figure 16: (a) Schematic diagram of the SQUID vibrating coil magnetometer. Experimental setup: (1) top flange of exchange gas chamber to fit the cryostat insert, (2) exchange gas

chamber, (3) sample holder, (4) heater coil, (5) sample, (6) superconducting (Nb–Ti) pick-up coil, (7) split-coil-type solenoid, (8) transmitting rod, (9) bimorph PZT actuator, (10) OFHC copper bottom, (11) brass ring, (12) SQUID assembly holder (material: phenolic resin bonded cotton fabric), (13) OFHC copper tube, (14) SQUID electronics board holder (material phenolic resin bonded cotton fabric), (15) SQUID device, (16) Pb shield—1.5 mm thick and (17) cryoperm shield—2.5 mm thick.

The pick-up coil of the SVCM is steadily vibrated at the resonant frequency with maximum amplitude of ~70 μm and it is kept close to the sample by three bi-morph piezoelectric bender type actuators. An equivalent circuit model for the piezoelectric actuator is also constructed and its resonance frequency is cross-checked by simulation software. The vibration of actuators is controlled by a negative feedback circuit for a wide range of temperatures (4.2 K – 300 K). It is possible to incorporate the diamond anvil cell with SVCM experimental setup for investigation of various materials under high pressure and low temperature. The experimental setup is shown in figure 16.

Establishment of low temperature, and high magnetic field facilities: Suits for transport and magnetic measurements.

We established the following equipments at Centre for High pressure Research, School of Physics, Bharathidasan University, Tirucirappalli-620 024 and various pressure devices/ cells suits very well for to do transport and magnetic \measurements at ambient and high pressures.

The Physical Property Measurements System (PPMS) - Vibrating sample Magnetometer:

The Physical Property Measurements System (PPMS) is a special equipment with variable temperature (2 – 400 K) and field (upto 9 T) that is optimized to do R(T) measurements at ambient and high pressure upto 3 GPa with the combination of 9T magnetic field. The developed hybrid hydrostatic piston-cylinder pressure cell suits to PPMS. The VSM option for the PPMS consists primarily of a VSM linear motor transport (head) for vibrating the sample and pickup coil for detection. For magnetization measurements at ambient pressure, the small bore is used, whereas the large bore coil is used for temperature dependence of magnetization at various clamped pressures using 1 GPa pressure cell. It is also possible to heat capacity measurements at ambient pressure.

PPMS - VSM (2K-400K 9T)

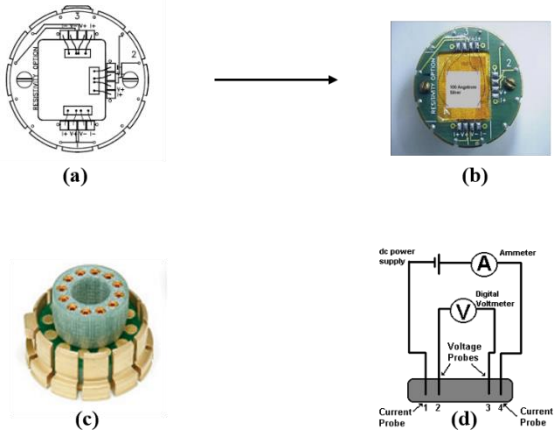

Figure 17. Photograph of a Physical Property Measurement system - Vibrating Sample Magnetometer (Quantum Design, USA) setup. **Figure. 18. a)** Resistivity sample puck, b) Front view of resistivity sample puck, c) Rear view of the sample puck, and d) Schematic representation of a four-probe method.

9T cryogen free superconducting magnet with an Integrated Variable Temperature Insert (IVTI).

The Cryogen-Free Measurement System (CFMS) from Cryogenic Ltd is a modular research platform designed to enable the user to perform a wide range of material characterisation experiments in variable field and variable temperature environments. The base system of every CFMS is made up of a 9T cryogen free superconducting magnet with an Integrated Variable Temperature Insert (IVTI). An automatic needle valve is available for ease of system control. Complementing this is a range of specifically designed measurement modules with associated electronics for magnetic, electrical, thermal property and ultra-low temperature measurements. Magnet configurations up to ±9 Tesla are available with a standard temperature range of 1.8 K – 400 K. Active shielding is available for magnets of 9 T and higher. The IVTI is made in such a way to suit for Hybrid hydrostatic piston cylinder pressure cell (3 GPa), Modified Bridgman Anvil pressure cell (8GPa) and Diamond Anvil Pressure Cell (20 GPa) for electrical resistivity measurements.

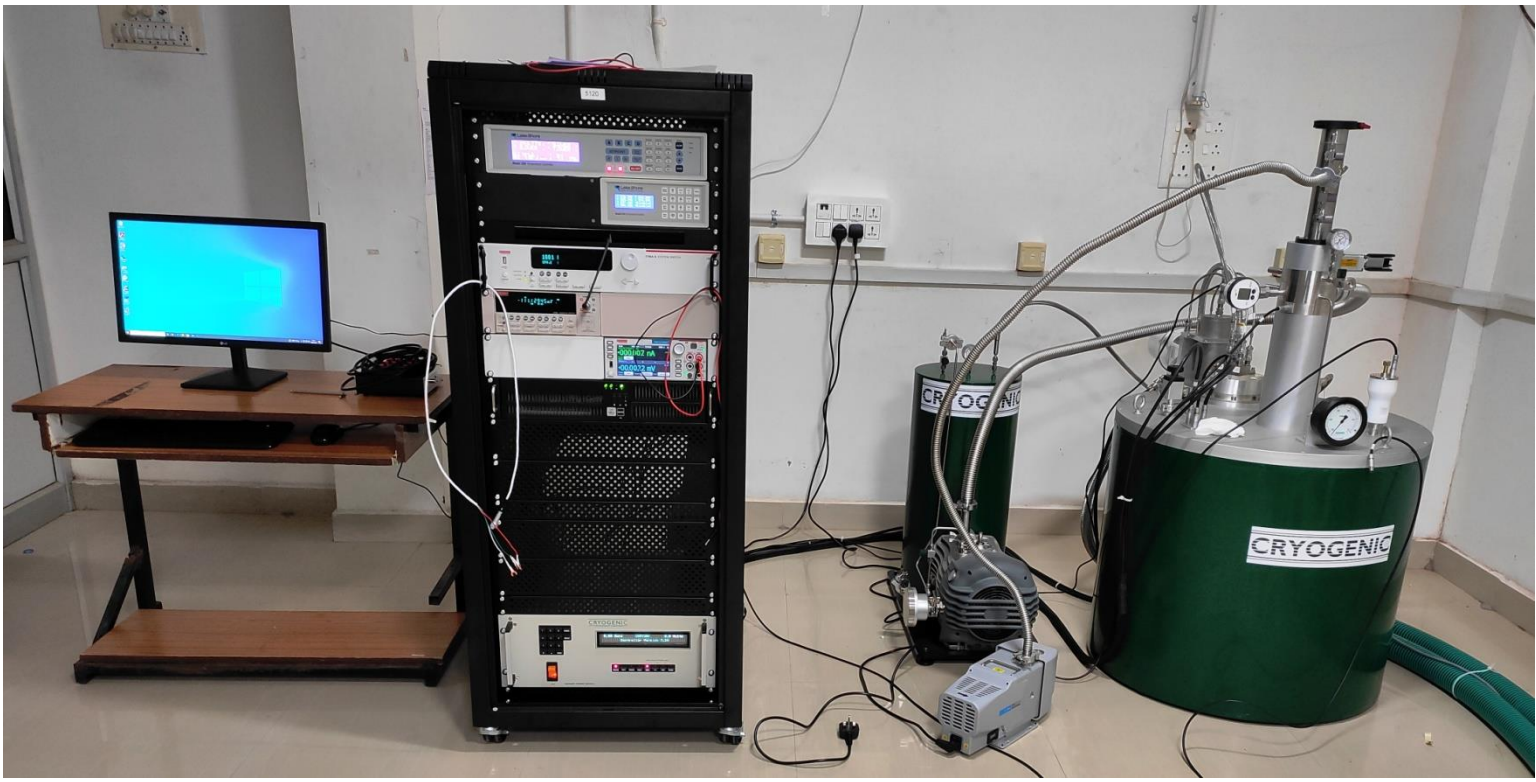

Figure 18. 9T cryogen free superconducting magnet with an Integrated Variable Temperature Insert (IVTI) (Cryogenics, UK) with measuring instruments and power supply for a magnet.

3.7.3.Cryogen free Closed Cycle Refrigerator – Variable Temperature Insert (CCR-VTI) system

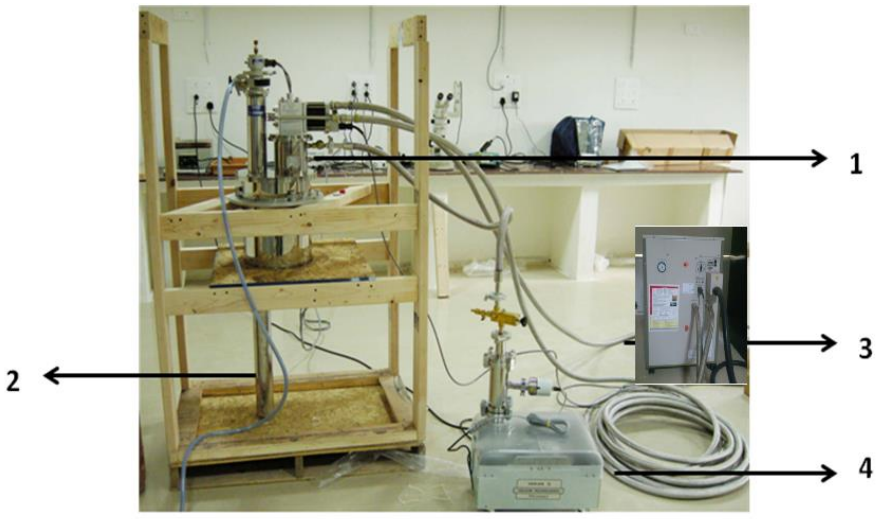

Figure. 19 Photograph of a Closed Cycle Refrigerator System - Variable Temperature Insert (Sumitomo, Japan) setup.Parts are noted in numerical order (1) cryostat chamber, (2) VTI, (3) compressor, (4) Turbo Molecular Pump.

Electrical resistance measurements are rather easy and straight forward to carry out and provide much useful information about the electrical properties of the sample. The

measurements of electrical resistance as a function of temperature to give information about the various temperature dependent of electronic phase transitions. The temperature dependence of electrical resistivity was measured using resistivity option and Cryogen free Closed Cycle Refrigerator – Variable Temperature Insert (CCR-VTI) system. The CCR-VTI is a cryogen free equipment to measure physical properties at low temperature down to 4 K. The CCR-VTI system consists of four major parts such as cryostat chamber (Cryo Industries, USA), VTI, compressor (Sumitomo, Japan) and Turbo Molecular Pump (Varian Industries, USA). The electricity resistivity measurements were performed under ambient and hydrostatic pressure in the temperature range of 4 – 300 K using CCR-VTI. . The data collection is indigenously automated with Lab View Software with temperature controller, nanovoltmeter, constant current source, temperature sensors and personal computer.

DAC for High Pressure XRD

Materials Synthesis facility:

The materials synthesis facility (solid state reaction method and sol gel method) is established and synthesized various materials such as five element alloys, eight element alloys, doped hexa ferrites, manganites, superconductors, Sensor and super capacitor materials by using muffle and tubular furnaces. The facilities are shown below:

Muffle Furnace (Technico, Chennai) upto 1200^{0}C

Muffle Furnace (Sandy Scientific, Chennai)upto 1500^{0}C

Vacuum Tubular furnace (Technicho, Chennai)

TubularFurnace (Technico, Chennai) upto1000^{0}C

100Ton (LYXN, Lawrence & Mayo) and 20 Ton (Riken Kiki, Japan), hydraulic press

Other Established Facilities @ CHPR

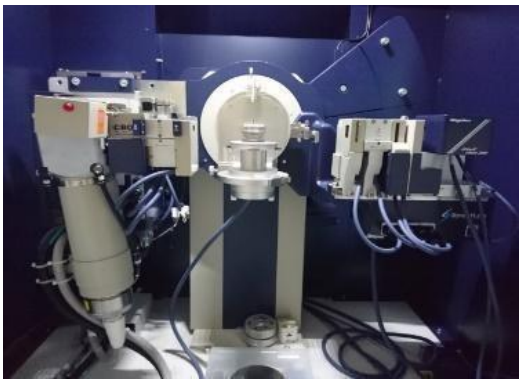

POWDER XRD

CNCLathe(Tutor)

B2901A

34420ANano

2401Source

4263BLCR

SR860DSP

Lakeshore 331

Research Contribution: Investigation of Strongly correlated materials under High Pressure:

Pressure effect on superconducting materials (Fe, BiS_2, Noncentrosymmetic and Topological Insulators)

Recently, we were working more sincerely to understand the 100 years question (relation between magnetism and superconductivity) of high T_c superconductors from few Fe, BiS_2 and Topological insulators based superconducting materials with respect to high pressure, high magnetic field and low temperature studies. We are to be near the answer but not exactly to say; but from the obtained results will give the clues for realize this critical phenomenon. However, we have obtained some interesting data's by application of pressure as well as low temperature. First, the $CeFe_{0.9}Co_{0.1}FeAsO$ shows the enhancement of T_c from 11.4 to 12.3 K with a small increase in pressure up to 0.4 GPa and it is first time observed in an electron doped Ce-1111 system. The anisotropic compression of c - axis we observed also may play an important role in determining the T_c in these layered superconducting compounds. A pressure induced structural change to a collapsed tetragonal structure is observed above 10 GPa at RT **(App. Phys. Lett. 2011)**. The application of external pressure increases the T_c to 31 K with a positive pressure coefficient of ~1 K/GPa and low temperature X-ray diffraction studies performed at 7.8 K at high pressures show no pressure induced structural changes were observed in Thorium doped $La_{1-x}Th_xFeAsO$ (x = 0.2) superconductor **(Phys. Status Solidi RRL. 2011)**. Pressure effects on $Ce_{0.6}Y_{0.4}FeAsO_{0.8}F_{0.2}$ shows the application of external pressure initially enhances the transition temperature (T_c) up to 1 GPa at a rate of 0.28 K/GPa. However on further increase of pressure above 4 GPa leads to a complete suppression of superconductivity where the change in compressibility of the tetragonal phase is observed with a transition to a collapsed tetragonal phase **(App. Phys. Lett., 2012)**. The drastic suppression of T_c at ~ 3 GPa may be either due to a pressure induced structural distortion, change of valence of Ce^{3+} or strong hybridization of Ce (4f) and Fe (3d) localized electrons, which is speculated to induce the Kondo screening effect. The Effect of pressure on the superconducting transition temperature (T_c) of Yb doped $Ce_{0.6}Yb_{0.4}FeAsO_{0.9}F_{0.1}$ has been investigated for the first time using resistivity and magnetization studies. Enhancement in T_c with external pressure has been observed for this compound up to a maximum value of T_c = 48.7 K at 1 GPa, beyond which T_c starts decreasing monotonously **(Phys. Status Solidi RRL., 2012)**. In addition, the effect of external pressure on T_c of as grown and annealed single crystals of iron chalcogenide $Rb_{0.85}Fe_{1.9}Se_2$ has been studied. The as grown sample a T_c of 27 K was found at ambient

pressure, whereas it is found to increase up to 33.2 K in the sample annealed at 215 ^{o}C in vacuum for 3 h. Thereafter, T_c of the as grown sample increases up to 28 K at a pressure of 0.83 GPa **(Phys. Status Solidi RRL., 2013)**. We have investigated the effect of applied pressure (P) on the magnetic and superconducting transitions of $GdFe_{1-x}Co_xAsO$ (x = 0, 0.1, 1) compounds by measuring the temperature dependence of resistivity. For the $GdFe_{0.9}Co_{0.1}AsO$ sample, the superconducting onset temperature T_c^{on} decreases monotonically from 19 to 17.1 K, and the temperature T_c^{zero} at which the resistivity disappears decreases from 16.7 to 10.5 K as pressure increases from 0 to 2.9 GPa. The strength of electron– electron correlation also decreases with increasing pressure. Both these effects arise due to the increase of bandwidth with pressure **(Supercond. Sci. Technol., 2015).**We have investigated the effect of pressure up to 8 GPa on both superconducting and normal state properties of optimally doped oxygen-deficient $PrFeAsO_{0.6}F_{0.12}$ sample in which sharp superconducting transition and large superconducting volume fraction are observed. With increase in pressure, T_c initially increases for pressure up to 1.3 GPa and then decreases. The Meissner signal shows a systematic increase with pressure up to 1.1 GPa. On the other hand, both T_c and Meissner signal are observed to decrease with pressure for over doped $PrFeAsO_{0.6}F_{0.14}$ sample. **(NatureScientific Reports Feb, 2017).**

Further, we are investigating recently discovered BiS_2 based superconductors with external hydrostatic pressure upto ~3 GPa for resistivity and ~ 1 GPa for magnetic measurements. The T_c is found to have a moderate decrease from 4.8 K to 4.3 K (–0.28 K/GPa) for $Bi_4O_4S_3$ superconductor and the same increases from 4.6 K to 5 K (0.44 K/GPa) up to 1.31 GPa followed by a sudden decrease from 5 K to 4.7 K up to 1.75 GPa for $NdO_{0.5}F_{0.5}BiS_2$ superconductor. The variation of *T*c in these systems might be correlated to an increase or decrease of the charge carriers in the density of states under externally applied pressure (**Phys. Status Solidi RRL. 2013)**. At ambient condition Critical current density (J_c), thermal activation energy (U_0), and upper critical field (H_{c2}) of $La_{1-x}Sm_xO_{0.5}F_{0.5}BiS_2$ (x = 0.2, 0.8) superconductors are investigated from magnetic field dependent ρ (T) studies. Our studies show that on substitution of smaller rare earth metal (Sm) in place of La in $LaO_{0.5}F_{0.5}BiS_2$ successfully improves and enhances magnetic flux pinning forces making this superconductor a potential candidate for superconducting applications **(J.Phys.Soc., 2015)**. At External pressure condition, the T_c in $La_{0.8}Sm_{0.2}O_{0.5}F_{0.5}BiS_2$ is increased from 3.2 K to above 10.3 K under pressure just above ~1.5 GPa for under doped compound. This is a dramatic (more than threefold) enhancement of T_c. The quality of the superconducting transition is also significantly improved under high pressure. In addition, there is a concomitant improvement

in the normal-state resistance and a suppression of the semi-metallic behavior of the material. While there is virtually no effect of pressure on the T_c of the $x = 0.8$ materials, there occur a transformation from semiconductor to metallic behavior in the normal state just as in the sample with $x = 0.2$ **(J. Phys. D: App. Phys., 2016).**The bulk superconducting properties of polycrystalline TaRh2B2 under pressure are investigated with transport resistivity [ρ (T)], and dc magnetization [M (T) and M (H)] measurements up to ~3 GPa, and 1 GPa respectively. The application of hydrostatic pressure leads to a decrease in Tc for both magnetic [$dTc/dP$is -0.4 K/GPa ($0 \leq P \leq 1$ GPa)] and transport [(dTc/dP) is -0.02 K/GPa ($0 \leq \Delta P \leq 1$ GPa) and -0.06 K/GPa ($1 \leq \Delta P \leq 2.5$ GPa)] measurements **(PHYSC-2019).**

The $Sr_xBi_2Se_3$ has been recently reported to be a superconductor derived from Bi_2Se_3 topological insulator. It shows a maximum superconducting transition temperature (T_c) of 3.25 K at ambient pressure. The T_c is found at 2.67 K at 0 GPa and its decreased upto 1.96 K (0.81 GPa) observed from magnetic measurements. Band structure analysis involving external pressure to $Sr_{0.1}Bi_2Se_3$ shows decrease in DOS at Fermi level with application of pressure. The suppression of T_c with increasing normal state resistivity and increasing electronic correlation is well accounted by decreasing N (E_F) as evidenced in conventional low T_c superconductors (**EPL-2017).**Temperature and field dependence of magnetic measurements under hydrostatic pressure are carried out on a noncentrosymmetric superconductor α-BiPd up to1 GPa, and a 3D (temperature—magnetic field—pressure) phase diagram is reported for the first time. The experimental results are analyzed using various theoretical approaches, such as the Ginzburg–Landau formula, Bean's critical state model, Dew–Hughes model, and collective pinning theory, and several superconducting parameters are also estimated. Critical temperature, critical current density, and pinning force are decreased with the application of both pressure and magnetic field. It is observed that pressure diminishes the superconductivity moderately and changes the mean free path, which leads to crossover from the δTc pinning mechanism to δl type in α-BiPd (**Phys. Status Solidi RRL 2019)**

The impact of hydrostatic pressure (P) up to 1GPa on *Tc*, *Jc*and the nature of the pinning mechanism in Fe_xNbSe_2 single crystals have been investigated within the framework of the collective theory. We found that the pressure can induce a transition from the regime where pinning is controlled by spatial variation in the critical transition temperature (δTc) to the regime controlled by spatial variation in the mean free path ($\delta\ell$) (**Scientific Reports (2018)**). Superconducting properties of $Cr_{0.0005}NbSe_2$ (Tc~6.64 K) single crystals have been investigated through the temperature dependent resistivity (~8GPa) and DC magnetization

(~1GPa) measurements. Further, the critical current density (*Jc*) as a function of applied magnetic field has been studied from magnetic isotherms. The vortex pinning mechanisms have also been systematically analyzed using weak collective pinning theory as a function of pressure. The *Jc* corresponds to the flux follow enhanced by the application of pressure due to increase of *Tc* and vortex changes (**Scientific Reports (2019))**. We investigated the superconducting critical current density (J_c), transition temperature (T_c), and flux pinning properties under hydrostatic pressure (P) for $Cr_{0.0009}NbSe_2$ single crystal. The application of P enhances T_c in both electrical resistivity (0.38 K GPa1: 0 # P # 2.5 GPa) and magnetization (0.98 K/GPa) measurements, which leads to a monotonic increase in J_c and flux pinning properties (**RSC Adv., 2020**). Effect of the weak point disorder on vortex matter phase diagram is studied by incorporation of V atoms through magnetic and magnetoresistance measurement in layered $NbSe_2$ single crystal. We observed that the point disorder introduces fishtail effect and the second magnetization peak (SMP) in the M-H curve of $V_{0.0015}NbSe_2$ at magnetic field far below upper critical field (H_{c2}) (**Journal of Magnetism and Magnetic Materials 507 (2020)).**

Pressure Effect on Manganites

Manganites offers a great degree of chemical flexibility allowing not only the substitution of different cations over a wide range of composition but also the introduction of vacancies or substitutions on the anion sublattice, which permits the relation between the structure, electronic and magnetic properties to be examined in a systematic way. An exciting physics is underlying not only in the ground state of manganites, but also in some of the excited states under different external parameters such as pressure, magnetic field and temperature. The most fundamental property of these materials is the strong interplay between lattices, charge and spin degrees of freedom. As a result of coupling between them, interesting physical effects take place when thermodynamic parameters such as pressure, magnetic field and temperature are varied. In manganites, pressure influences the electrical conducting properties as well as the interaction responsible for FM. Thus investigation under pressure may give further information about the delicate balance between structure, magnetism, and electron mobility. So, based on these phenomena, we have interested to carry out the experiments to study the influence of hydrostatic and uniaxial pressure on various perovskite and bilayer manganites are summarized as follows:

We have carried out a systematic investigation on magnetic and transport properties under extreme conditions of high pressure, low temperature and high magnetic field of bilayer manganites such as $Pr(Sr_{0.6}Ca_{0.4})_2Mn_2O_7$,$(L_{0.4}Pr_{0.6})_{1.2}Sr_{1.8}Mn_2O_7$, and Perovskite manganite such as $Sm_{0.55}(Sr_{0.5}Ca_{0.5})_{0.45}MnO_3$, $La_{0.4}Bi_{0.3}Sr_{0.3}MnO_3$, $Pr_{0.6}Ca_{0.4}Mn_{0.96}B_{0.04}O_3$ (B=Co and Cr). Analysis of magnetization data on $Pr(Sr_{0.6}Ca_{0.4})_2Mn_2O_7$ reveals only one charge-orbital ordering (CO-OO) transition occurs which decreases very slowly with pressure, while the antiferromagnetic ordering transition shifts towards higher temperature with the increase of pressure**.** A huge negative piezoresistance in the low temperature region with insulator to metal transition at moderate pressures is observed in $(L_{0.4}Pr_{0.6})_{1.2}Sr_{1.8}Mn_2O_7$ and $Sm_{0.55}(Sr_{0.5}Ca_{0.5})_{0.45}MnO_3$ samples. Moreover, a first to second order phase transition is observed in $La_{0.4}Bi_{0.3}Sr_{0.3}MnO_3$ at 0.91 GPa in M (T), and $Pr_{0.6}Ca_{0.4}Mn_{0.96}B_{0.04}O_3$ (B=Co and Cr) at 2.02, 2.40 GPa in ρ(T). The critical behavior of second order phase transition under pressure of the samples is analyzed. Recently, have studied the pressure effect on spin re-orientation transition on La doped $Sm_{0.7-x}La_xSr_{0.3}MnO_3$manganties, observed the suppression of spin reorientation only on La doped system along metal-insulator transition. In one more well-known manganite system $NdMnO_3$ shows re-entrant of first-order transition the suppression of the temperature spin glass transition the doping of Cd at Nd site for 0.3 compositions. Till date we have published =24 International peer-reviewed journals.

Pressure effects on Ni-Mn based Heusler alloys

The pressure plays a crucial role in modifying the Mn-Mn bond length which is responsible for the observed magnetic behavior in the $Ni_{50-x}Mn_{37-x}Sn_{13}$ alloys. The effects of Cu substitution on structure, magnetic, martensitic, and intermartensitic transformation in $Ni_{49-x}Cu_xMn_{38}Sn_{13}$ Heusler alloys are investigated. The substitution of Cu for Ni results in decrease of lattice parameter due to the smaller atomic radii of Cu. The substitution of Cu introduces an intermartensitic transformation, which vanishes for high content of Cu. The observed intermartensitic transformation vanishes with the application of both external magnetic field and hydrostatic pressure. The magnetization of both the austenite and martensite phases decreases with the increase of pressure. The increase in the Ms Value toward room temperature and the nominal decrease in ΔS_m with pressure make the x =2 alloy a potential candidate for magnetic refrigeration applications. The hydrostatic pressure effects on martensitic, magnetic and magnetocaloric effect in the $Ni_{48}Mn_{39}Sn_{13-x}Si_x$ (x = 1 and 4) alloys are investigated. We inferred that the structural transition temperature increases linearly with respect to external pressure and decreases with the application of magnetic field. A large increase in ΔS_m has been

observed for x = 1 alloy, whereas it decreases for x = 4 alloy. However, the peak temperature of ΔS_m is shifted towards higher temperature with the application of pressure for both x = 1 and 4 alloys. The observed pressure effects on refrigeration capacity is found to increase for x = 1 alloy and decrease for x = 4 alloy. Advantage of having high ΔS_mandRC_{eff}value with respect to pressure, makes the $Ni_{48}Mn_{39}Sn_{13-x}Si_x$ (x = 1) alloy as a potential candidate for the application of magnetic refrigeration.

We report here on the temperature- and field- dependence of resistivity measurements of $Nd_{1-x}Cd_xMnO_3$ (x = 0 and 0.1) polycrystals and compare them with the magnetization measurements on the same set of samples reported earlier. A transition from an anti-ferromagnetic insulator to a ferromagnetic insulator is observed for x = 0.1. Magnetic entropy change of both the samples around semiconducting to insulating transitions have been estimated using magnetization and resistivity measurements for the first time. The values for x = 0 and 0.1 samples are 45 $J.kg^{-1}.K^{-1}$and 63 $J.kg^{-1}.K^{-1}$ respectively for a magnetic field difference of 5 T indicating an enhancement as increases from x = 0 to 0.1. The activation energy (E_a) and density of states at the Fermi level[$N(E_F)$] are estimated for both the samples using small polaron hopping and two dimensional variable range hopping models respectively (**JMMM-MAGMA -2018**).

We report the effect of Fe on the martensitic transitions in $Ni_{47}Mn_{40-x}Fe_xIn_{13}$ (x = 1 and 2) alloys and associated magnetocaloric effect. Structural and magnetic transitions are observed in x = 1 and 2 alloys. The martensitic transition shifts to low temperature with the increase of Fe concentration. The maximum positive entropy change (ΔSM) with quite large magnitude of 22 $Jkg^{-1}K^{-1}$ (x = 1) and 51.2 $Jkg^{-1}K^{-1}$ (x = 2) are observed for a field change of 50 kOe. Substitution of Fe enhances the magnetization as well as increases the Δ_{SM} more than a twice in the x = 2 system (**Journal of Magnetism and Magnetic Materials (2018)**).

Non-oxide NiF_2 and MnF_2system as a best supercapacitor Materials:

We report here on the complex magnetic structure and magnetocapacitance in NiF2, a non-oxide multifunctional system. It undergoes an anti-ferromagnetic transition near 68.5 K, superimposed with canted Ni spin driven weak ferromagnetic ordering, followed by a metastable ferromagnetic phase at or below 10 K. Our density functional calculations account for the complex magnetic structureofNiF2 deduced from the temperature and the field dependent measurements. Near room temperature, NiF2 exhibits a relatively large dielectric response reaching >103 with a low dielectric loss of <0.5at frequencies >20 Hz. This is

attributed to the intrinsic grain contribution in contrast to the grain boundary contribution in most of the known dielectric materials. The response time is 10 μs or more at280 K. The activation energy for such temperature dependent relaxation is ~500 meV and is the main source for grain contribution. Further, a large negative magneto capacitance >90% is noticed in 1Tmagnetic field. We proposed that our findings provide a new non-oxide multifunctional NiF2, useful for dielectric applications (Scientific Reports -2019, Materials Letters 2020 and J.Electro Analytical Chemistry 2020)